Food Hydrocolloids 137 (2023) 108399

Contents lists available at ScienceDirect

Food Hydrocolloids

journal homepage: www.elsevier.com/locate/foodhyd

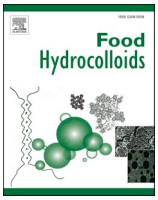

Tunable oleosome-based oleogels: Influence of polysaccharide type for polymer bridging-based structuring

Juan C. Zambrano, Thomas A. Vilgis *

Max Planck Institute for Polymer Research, Ackermanweg 10, 55128, Mainz, Germany

ARTICLE INFO

Keywords:
Emulsions
Bridging
Oil structuring
Oleosomes
Polysaccharides
Electrostatic interactions

ABSTRACT

This research proposes a gelation method using soybean oleosomes as templates in combination with polysaccharides. Two anionic polysaccharides, sodium alginate, and xanthan gum were investigated for their ability to induce bridging flocculation. Bridging flocculation occurs when flexible polysaccharides such as alginate strongly interact with oppositely charged oleosome particles in acidic pH ranges. In contrast, the more rigid xanthan leads to a different flocculation mechanism, which is not driven by strong electrostatic attractive interactions. In microscopy images, xanthan induced microscopic and macroscopic phase separation between oleosome droplets and xanthan, presenting large, irregular-shaped particles. The ratio between alginate chains and oleosome droplets is critical for optimum bridging, where 0.005 g/g (also expressed as an equivalent per droplet surface area 0.4 mg/m^2) induced extensive droplet flocculation. It is possible to obtain an interconnected droplet network at this optimum ratio. Upon densification at the optimum ratio, a compact and self-supporting gel of about 46 wt% starting from 5 wt% oleosome is obtained. Oscillatory rheology showed that gels at optimum bridging ratio have higher moduli (G') than those formed at a different ratio, confirming a highly cross-linked network. Bridging flocculation provides an alternative method to design gels with predictable rheological properties suitable for food and drug design and cosmetic applications.

1. Introduction

The addition of polysaccharides to charge-stabilized emulsions significantly affects the structural arrangement of emulsion droplets. For instance, polysaccharides can induce oil droplet aggregation by a bridging flocculation mechanism. Bridging flocculation occurs under a certain range of polysaccharide concentration, where single polymeric chains can link two or more neighboring oil droplets, eventually leading to a particle gel network (T. B. Blijdenstein, Van Winden, et al., 2004a,b; Jiang et al., 2021). Furthermore, bridging flocculation takes place when polysaccharide molecules have a strong affinity for the droplet interface. This affinity generally results from attractive electrostatic interactions, as shown in protein-stabilized emulsions flocculated by polysaccharides (Dickinson & Pawlowsky, 1997; Zhai et al., 2021). Bridging flocculation can be used as a structuring process to controlled design of soft materials. For instance, the molecular weight, charge density, and conformational structure of the chosen polysaccharide will influence the effectiveness of a polymer in inducing bridging flocculation (Yu & Somasundaran, 1996; Zhai et al., 2021; Zhou & Franks, 2006). The present papers studies in detail the flocculation mechanism of sodium alginate and xanthan gum, which vary significantly in their structural configuration despite being both negatively charged. The polymeric chains of sodium alginate are composed of a random sequence of D-mannuronic acid (M), and L-guluronic acid (G) blocks combined with regions of alternating MG blocks. The occurrence and combination of these blocks influences the stiffness or flexibility of the polymer chain (Hu et al., 2021). The structure of xanthan gum consists of repeating units of 1, 4-linked β-D-glucose with side chains containing two mannose units separated by guluronic acid. The negatively charged carboxyl groups on the side chains of the molecule are responsible for a very stiff, rod-like backbone that results in unusual and functional properties such as a high degree of solution pseudoplasticity (Vilgis, 2015). Therefore, the structural differences between sodium alginate and xanthan gum will provide tunable physical properties of the flocculated emulsions and resulting oleogels.

For sustainable and economic reasons, using natural templates, such as oleosomes, for complexation with polysaccharides has emerged as a potential alternative to traditional 'artificial' emulsions. Oleosomes are

* Corresponding author.
E-mail addresses: zambrano@mpip-mainz.mpg.de (J.C. Zambrano), vilgis@mpip-mainz.mpg.de (T.A. Vilgis).

https://doi.org/10.1016/j.foodhyd.2022.108399
Received 22 September 2022; Received in revised form 29 November 2022; Accepted 7 December 2022
Available online 14 December 2022

naturally pre-emulsified oil droplets in oleaginous seeds and nuts such as soybeans, sunflowers, and hazelnuts. Because of the charged nature of its surface, it is possible to bind to oppositely charged polysaccharides. Oleosin, the primary structural protein, is one of the endogenous surface proteins contributing to this charged nature. Oleosin comprises a hydrophilic *N*-terminal, a *C*-terminal facing the continuous water phase, and a lengthy hydrophobic domain firmly fixed in the triacylglycerols (TAGs) core (Nikiforidis, 2019). Oleosins are deeply embedded within a monolayer membrane of phospholipids surrounding the inner core TAGs (Nikiforidis, 2019). Although many previous studies have proved polysaccharides' complexation with oleosomes via electrostatic interactions (Su et al., 2018; Yang et al., 2020; Zielbauer et al., 2018), studies have yet to focus on the effect of anionic polysaccharides on bridging flocculation of oleosomes. Therefore, this study focuses on systems containing soybean oleosomes, sodium alginate, and xanthan gum under conditions favoring electrostatic interactions. For this purpose, the pH values will be gradually lowered to values where both oleosome and polysaccharide are opposite charged. As a result, the zeta potential was measured, the particle size was characterized, and the contraction rates of the network (v) were calculated during demixing experiments. These experiments have been combined with microscopy visualization and rheology.

2. Materials and methods

2.1. Materials

Commercially available soybeans was purchased from Rapunzel Naturkost GmbH (Legau, Germany) and were used for the extraction of oleosomes. Sodium alginate (TICA-algin 400 Powder) was provided by TIC Gums, Inc. (Belkamp, Md., USA). Xanthan gum extra pure was provided by Carl Roth (Karlsruhe, Germany). Distilled water was used for the preparations of all solutions.

2.2. Sample preparation

Soybean oleosomes extraction is based on the method described by Waschatko et al., 2012. Soybeans were soaked in distilled water at 4 °C for at least 20 h. Then water was added to obtain a 10% soybean-to-water ratio, grounded in a Vorwerk Thermomix TM31 at 10.200 rpm for 90 s at 25 °C. The resulting slurry was filtered through two layers of Kimtech wipes 21 × 11 cm (Kimberly Clark) to obtain raw milk. 25 wt% Sucrose was added to the raw milk and the pH was adjusted to 11.0 with 1 N NaOH (VWR Chemicals) solution. The solution was filled with 50 ml centrifuge tubes (Roth), which were centrifuged at 15000×*g* at 4 °C for at least 5 h. The resulting floating fractions (cream layer) were collected with a small spoon and re-suspended in a new centrifuge tube in 45 ml of 20 wt% Sucrose in distilled water (pH 11.0). A new washing and centrifugation step (15000×*g*, 4 °C, 5 h) was repeated, and the resulting oleosome cream was collected in a centrifuge tube. This method removes unspecific bounded soybean storage proteins (glycinin and β-conglycinin) and other allergenic proteins (Gly m BD 30 K) from the surface of the oleosomes (Waschatko et al., 2012). The final oleosome content was determined by a halogen dryer and ranged between 50 and 60 wt%. Since the precise composition of oleosomes is unknown, Huang's (Huang, 1992) theoretical values from a geometry-based model are described. This model calculates the amounts of approximately 3.3% (w/w) phospholipids, 5.2% (w/w) protein, and 91.5% (w/w) triglycerides for an oleosome with a 0.350 μm diameter.

Depending on the nature of the experiments, oleosomes emulsions were diluted with distilled water (w/w) to the desired concentration. The initial pH value was adjusted to 7.0 with 1 NaOH. Dried Sodium alginate and Xanthan gum samples were added directly to the oleosome emulsion at different concentrations to form different mass ratios (gr Polysaccharide/gr Oleosome). Polysaccharides-oleosome mixtures were stirred for a minimum of 20 h at 25 °C to ensure proper hydration. Afterward, polysaccharides-oleosome mixtures were slowly adjusted to pH 4.0 via dropwise addition of HCl with varying concentrations (1.0, 0.5, 0.1, 0.01 N) at a constant stirring speed of 450 rpm. Samples were prepared in stock, some samples were used immediately for further experiments, and other sets of samples were centrifuged (at 5000×*g*, 4 °C, for 20 min) for separation and densification of flocculated oleosome droplets.

2.3. Demixing experiments

Immediately after being adjusted to pH 4.0, 5 wt% oleosome emulsions mixtures with alginate and xanthan containing various concentrations in the range 0–0.125 wt% were stored quiescently in a sealed glass tube at 25 °C. Demixing was monitored over 18 days by visually following the height of the cream layer as it demixes out of a serum layer. The emulsion samples' initial height, H_0, was 10 ± 0.8 cm. The height of the contracting network at time t was defined as $h(t)_{=}H(t)_{/}H_0$. Parameters were obtained from the demixing curves. The rate at which the network contracts was determined by using $= \Delta H_{(t)}/\Delta t$. Permeability coefficient B was determined by Darcy's law $v = BP(\eta H_0)^{-1}$ (Payne et al., 2001), where η is the viscosity of the aqueous phase. The pressure (P) is the pressure exerted on the emulsion droplet network due to density difference is given by $P = \Delta\rho g H_0\, \varphi$ (T. Blijdenstein, Van Winden, et al., 2004a,b), where $\Delta\rho$ is the density difference between the oil and aqueous phase, g is the acceleration due to gravity and φ is the volume fraction of oil. Delay time, t_{delay}, is defined as the time when network compression starts.

2.4. Particle size measurements

Freshly pH-adjusted emulsions were diluted in a ratio of 1:10 to obtain a final droplet concentration of 5 wt% using buffer solution (same pH 4.0 as the sample being analyzed) to avoid multiple scattering effects. The particle size distribution of the emulsions was determined as differential volume by using a laser diffraction particle analyzer (LS 13320 Beckmann Coulter, California, USA). Measurements were performed using a laser diode with λ = 780 nm and three Polarization Intensity Differential Scanning (PIDS) wavelengths at λ = 450, 600, and 900 nm. The data were analyzed using the instrument software applying Mie theory (Eremin, 2004) and using refracting indexes as follows: refractive indexes soybean oil and water 1.47 and 1.33, respectively. A few drops of emulsion were placed into the sample chamber of the instrument and then recirculated through the optical measurement cell. The mean particle size was reported as the volume-weighted value, d_{43}. Results were reported as the average of three measurements.

2.5. ζ-Potential measurements

Oleosome emulsions from concentrated stock were diluted to a concentration of 0.2 wt%, and the same procedure as 2.2 was repeated (polysaccharide addition, pH adjustment to 4.0) while maintaining the same oleosome-polysaccharide mass ratios from the other experiments. Diluted emulsions were injected directly into the measurement chamber of a particle electrophoresis instrument (Malvern Zetasizer Nano Z) that measures the direction and velocity of droplet movement in the applied electric field. An individual ζ-potential measurement was determined from the average of 3 readings taken on the same sample.

2.6. Microscopic imaging

Freshly pH-adjusted 5 wt% polysaccharides-oleosomes mixtures were observed by optical microscopy using a Carl Zeiss Axio Scope. A1 microscope (Carl Zeiss AG, Oberkochen, Germany). Images were captured using transmission bright field microscopy with the objective lenses magnifying 10 × at 25 °C. ImageJ software was used to insert the

scale bar. A drop of the emulsion was placed on a microscope slide and then covered with a cover slip. Confocal laser scanning microscopy (CLSM) was used to analyze network structure of flocculated oleosome/polysaccharide mixtures. CLSM was performed using a Zeiss Axiovert 200 M (Oberkochen, Germany). A few drops of Nile Red, a fluorescent label excited at 543 nm with a Helium–Neon laser, were added to stain the oil core of the oleosome droplets. 500 μL of the different mixtures were placed inside 8 well-chambered borosilicate coverglass systems (Nunc Lab-Tek, Thermo Fisher Scientific, USA). The obtained CLSM images were analyzed using the "ImageJ" software package.

2.7. Rheology measurements

After centrifugation, oscillatory rheology was performed on the compacted flocculated polysaccharide-oleosome mixtures to investigate their resulting viscoelastic properties. Measurements were performed with a Bohlin Instruments Gemini 200 rheometer (Malvern Panalytical Ltd., Malvern, UK) equipped with a 25-mm parallel plate geometry. The gap size was adjusted stepwise to the thickness of the gels until the load in the force was detected, leading to gap sizes between 1000 and 1500 μm. After loading, a 5-min waiting period at 25 °C was used to allow the sample's structure to relax before the measuring process began. Oscillatory amplitude sweeps were performed by increasing the strain logarithmically from 0.01 to 1000% at 1 Hz. All measurements were performed in triplicate at 25 °C from different batches of gels, and all samples were prepared individually.

2.8. Characterization of polysaccharides

The molecular conformation of Sodium alginate and Xanthan gum was determined by gel permeation chromatography combined with multi-angle light scattering (GPC-MALLS). Polysaccharides were dissolved in 0.1 M $LiNO_3$ at 25 °C. Measurements yielded distributions of molecular mass, M_w, and radius of gyration, R_g. In addition, ζ-potential values at pH 7.0 by dissolving both polysaccharides in a phosphate buffer. Averages are given in Table 1.

3. Results and discussion

3.1. Influence of pH on polysaccharides adsorption

The interactions between the different polysaccharides and the oleosome surfaces were investigated by ζ-potential measurements. The surface charge of bare oleosome droplets changed from −46.07 mV to +39.07 mV when the pH was decreased from 7.0 to 3.0 (Fig. 1). The net charge was near zero somewhere between pH-values of 4.0 and 5.0, close to the isoelectric point (pI) of the oleosome-associated proteins being oleosin the predominant one (Qi et al., 2017). Alginate and xanthan gum (Table 1), are considered anionic polysaccharides since they present negative charges at all the studied pH values considering their p*K*a values are above 3.0 (Bastos et al., 2018).

Adding polysaccharides to the oleosome droplets caused a change in charge density depending on whether alginate or xanthan gum was added. At pH values between 5.0 and 7.0 and a low concentration of polysaccharide (0.0001 wt%), alginate and xanthan had no significant effect on the oleosome net charge. Both polysaccharides and oleosome droplets are negatively charged at these higher pH values. In addition, a low amount of polymer chains was available to bind the droplet surface, preventing a significant change in the oleosome charge density. However, at pH 4.0 (where both polysaccharides and oleosomes are oppositely charged), a slight decrease in oleosome net charge starts with 0.0001 wt% alginate (from +25.63 mV to +10 mV).

On the contrary, xanthan does not significantly reduce oleosome net charge in these conditions. This observation suggests that alginate molecules can coat oleosomes, even at small concentrations, whereas xanthan molecules cannot. The relatively rigid xanthan molecules are unable to bend sufficiently to coat oleosomes and neutralize surface charges, as will be discussed in more detail later. Consequently, the gain in energy by adsorption cannot compensate for the entropy loss. In contrast, the uncharged blocks of alginate show high flexibility, and the distant charged blocks along the contour can adsorb partially on the surfaces of the oleosomes.

At higher concentrations of polysaccharide (0.005 wt%), alginate significantly affected the oleosome net charge, which increased from −46.07 to −54.03 mV at pH 7.0. Despite presenting similar charges at neutral conditions, polysaccharide molecules seem to adsorb to the oleosome surface. This can be explained by electrostatic interactions between anionic carboxylate groups (–CO_2–) on the alginate molecules and local cationic amino acid groups on the oleosome-associated proteins. A similar electrostatic interaction has been reported between anionic polysaccharides of high charge density and oil-in-water emulsions (Dickinson & Pawlowsky, 1998). The most significant change occurred at pH 4.0 where charge reversal of oleosome net charge followed (from +25.63 to −43.06 mV). The ability of anionic polysaccharides to bind to the surface of oppositely charged colloidal particles and cause charge reversal is well established in the literature (Bertsch et al., 2019). Consequently, alginate molecules strongly bind to numerous binding sites in the oleosome droplet interface via electrostatic interactions at higher alginate concentrations. The ratio between the chain length, flexibility, and surface curvature, determined by the oleosome radius, substantially influences polymer chain conformation to the surface of the oleosomes. The diameter of the oleosomes averages about 350 nm, as recently confirmed by small-angle neutron scattering (Zielbauer et al., 2018). As stated in Table 1, the squared average of the radius of gyration of alginate is about $R_g = 62$ nm. It is assumed that alginate chains are in a good solvent, $R_g \approx bN^{3/5}$, where b describes a statistic segment, and N corresponds to the degree of polymerization (De Gennes, 1979). This assumption is based on the absence of detailed information about the distribution of charged guluronic and uncharged mannuronic acids. Considering the guluron and mannuron monomers of the alginate, it can be assumed that b is on the order of 5 nm, indicating values of N of the order of 70 and an average chain length of 360 nm. Comparing the chain length with the diameter of the oleosome shows that the average chain can adsorb at the surface at more than one charged block.

On the other hand, xanthan at 0.005 wt% only slightly decreased oleosome net charge to +11.23 mV at pH 4.00. This suggests that xanthan adsorption to the oleosome droplet surface occurred to a small extent and was not significant enough to cause charge reversal of the oleosome net charge. In several studies, xanthan gum is considered a non-adsorbing polysaccharide, which does not bind to protein-stabilized droplet surfaces despite having negative charges along its chain (Boonlao et al., 2020; Moschakis et al., 2006). The physical reasons for these observations are clear. As mentioned before, xanthan shows high chain rigidity and must be considered as stiff polyelectrolyte (Sato et al., 1990). Its high bending energy is caused by steric and electrostatic reasons. Each monomer can dissociate a cation and becomes negatively charged. The charged monomers repel each other intensely, stiffening the chains electrostatically in addition to steric reasons (Wang & Wang, 2013).

Consequently, xanthan chains are far less flexible (and turn for energetic reasons into single helices) (Moorhouse et al., 1977). Their persistence length is, therefore, of the order of the total contour length. In practice, the measured gyration radius (Table 1) can be assumed to be

Table 1
Molecular characterization of alginate and xanthan. Surface charged expressed by zeta potential measurements at pH 7, R_g is the radius of gyration.

Polysaccharide	Surface charge (mV)	R_g (nm)
Sodium alginate	−55.19 ± 8.29	62
Xanthan gum	−29.24 ± 8.97	150

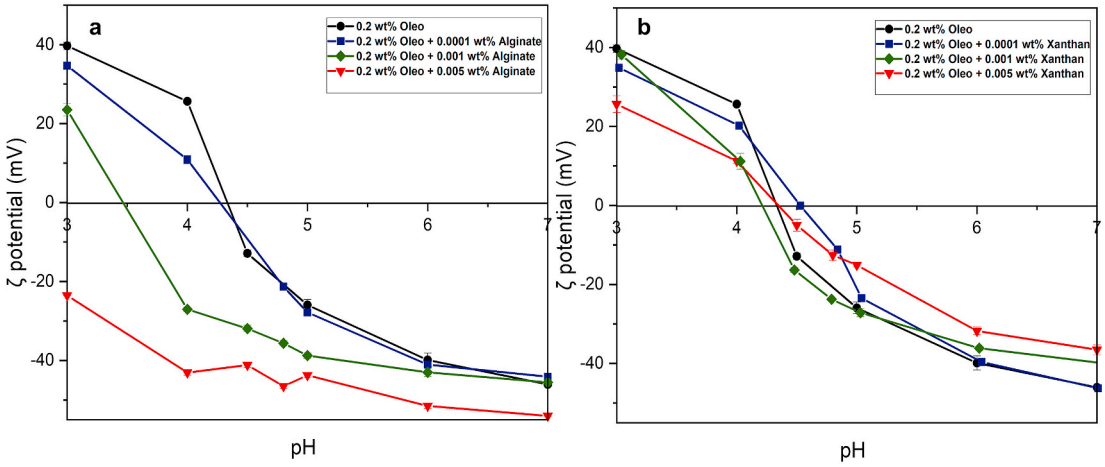

Fig. 1. Influence of pH on the ζ-potential of polysaccharide/oleosome mixtures a) 0.2 wt% Oleosome + Sodium Alginate b) 0.2 wt% Oleosome + Xanthan gum.

that of stiff rods. The interaction range scales as exp $(-r/\xi)/r$, where r is the distance between the charges, ξ is the electrostatic screening length, which depends on the total ionic strength. According to the previous expression, xanthan may adsorb only at a minimal number of monomers. As a result, the gain in electrostatic energy is low (Cheng & Olvera de la Cruz, 2003). It cannot balance the loss in entropy of free semi-flexible polyelectrolytes in solution, as outlined in Fig. 2.

Therefore, alginate has a stronger effect on the ζ-potential, even at low concentrations. The adsorption of the negatively charged guluron blocks neutralizes more of the positive charges of the oleosome surface proteins. On the contrary, xanthan has a lesser effect on adsorption. Interactions between xanthan gum and oleosomes may have taken place, but they seem not predominant enough, even under pH values where both xanthan and oleosome surface proteins are oppositely charged. Nevertheless, another study revealed (Nikiforidis & Kiosseoglou, 2010) that attractive electrostatic interactions were present between xanthan gum and maize oleosomes. This can be easily explained with similar ideas. Maize oleosomes are, on average, larger (Ting et al., 1996; Tzen et al., 1993), which makes the curvature of the oleosome surfaces appears flatter. Therefore, the overall interaction is more significant since rigid xanthan molecules can adsorb easier when the curvature radius comes of the order of the xanthan persistence length. This behavior will be essential to interpret the flocculation experiments in more detail, as shown below.

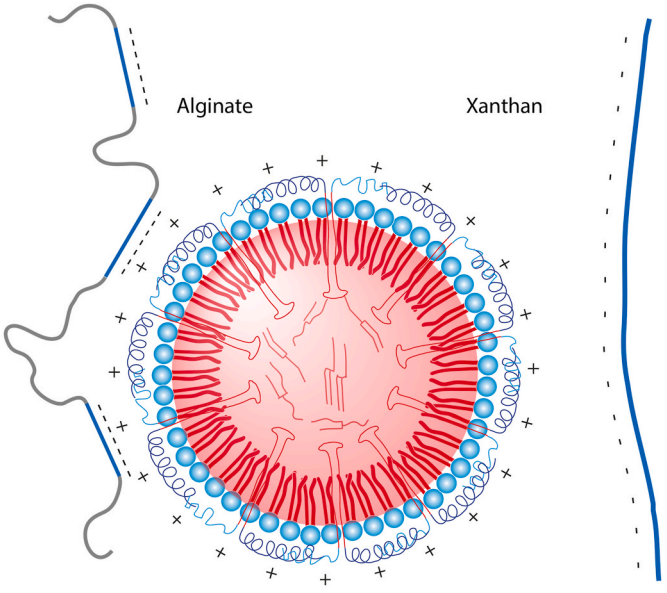

Fig. 2. Flexible alginate chains gain more energy when adsorbing on oppositely charged surfaces as semi-flexible, practically stiff xanthan molecules. Xanthan adsorbs with much lower probability, (free) energy and entropy are off balance due to high internal stiffness of the xanthan molecules.

3.2. Flocculation characterization of polysaccharide-oleosome mixtures

3.2.1. Demixing behavior and microstructural properties

The demixing kinetics of oleosome emulsions with alginate and xanthan gum were studied using plots showing the contraction of the network over time. Fig. 3a, b shows the visual appearance of oleosome at 5 wt% with different concentrations of alginate and xanthan (0.0025 wt %- 0.125 wt%) after being adjusted to pH 4.0. In the absence of polysaccharides (Fig. 3c), oleosome emulsion appears relatively stable until approximately 10^3 min, when the cream height decreases. Eventually, a steep decrease in cream height at 15^3 min occurs. In microscopy pictures (Fig. 5a), oleosome droplets appear homogenous with no signs of flocculation, with a small peak (0.350 μm) corresponding to intact oleosome droplets. However, a more prominent peak around 4.66 μm suggests the presence of single small flocs. It could be that single flocs where formed when the oleosome surface charge was reduced towards its isoelectric point (~pH 4.5). As a result, these small flocs slowly rise under gravity to the top of the emulsion, possibly dragging along most of the single unflocculated droplets and leaving behind a clear supernatant.

When polysaccharides are added to oleosome emulsions, a characteristic change in demixing behavior can be observed. The addition of alginate leads to extensive demixing of oleosome emulsion to a concentration up to 0.025 wt%, which further re-stabilizes at higher concentrations (Fig. 3a). The rate of network contraction v was extracted from the demixing curves. Fig. 4 shows a maximum in v (18.33 mm/h) at 0.025 wt% alginate. The maximum v indicates that extensive aggregation, associated with polymer bridging, already occurred during mixing and pH adjustment. This aggregation is likely to be driven by electrostatic interactions, as observed in Fig. 1a, where strong binding between alginate polymer chains and oleosome surface occurs at pH 4.00. Shortly after mixing, the rate of network contraction under gravity is mainly determined by the permeability of the network (T. Blijdenstein, Van Winden, et al., 2004a,b). Table 2 shows permeability coefficient, B, where 0.025 wt% alginate, presents the highest B. Microscopic images in Fig. 5c show a droplet network consisting of large and heterogeneous structures which may be responsible for large pores between the clusters and hence the higher initial permeability. Despite the high values for the rate v, the network height in 0.025 wt% alginate remained relatively unchanged at longer times (Fig. 3c). This indicates characteristics of a droplet network, which provides elastic resistance against

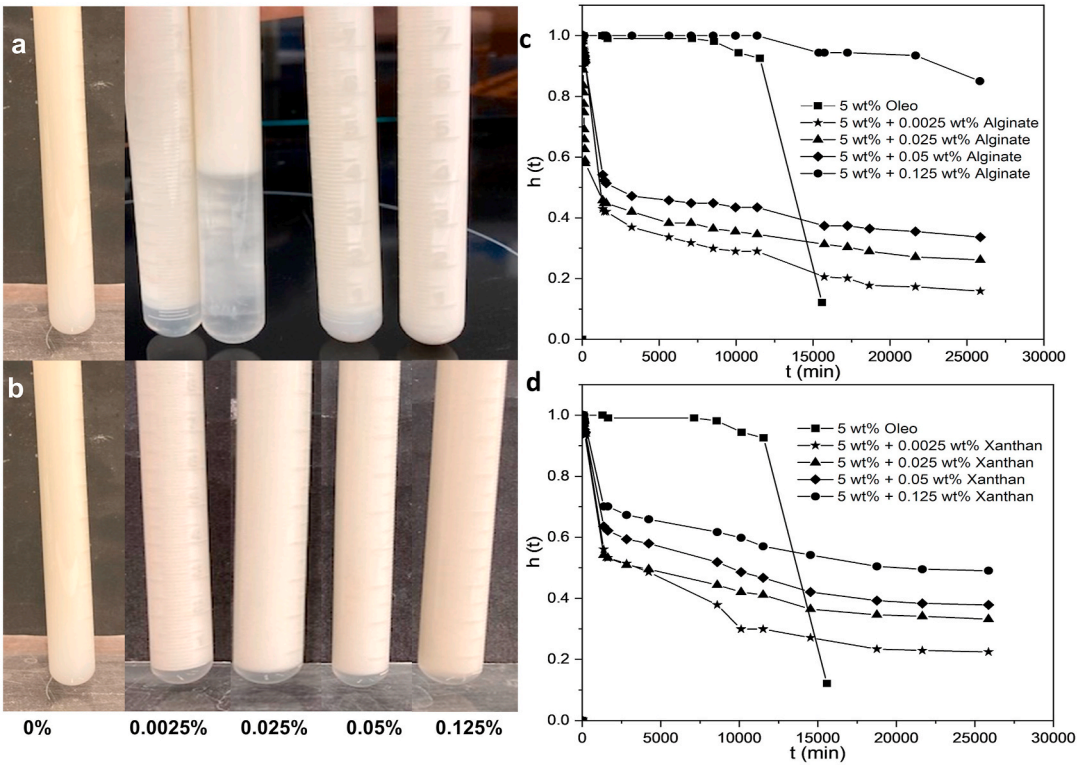

Fig. 3. Demixing experiments of 5 wt% Oleosome with different polysaccharide concentrations after being adjusted to pH 4. a) Visual appearance of alginate-containing mixtures b) Visual appearance of Xanthan-containing mixtures c) Plot of network height, $h(t)$, versus time of alginate-containing mixtures d) Plot of network height, $h(t)$, versus time of xanthan-containing mixtures.

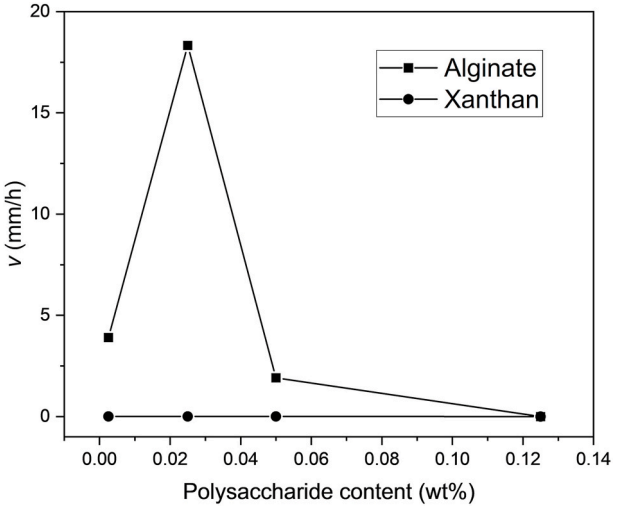

Fig. 4. Plot of network contraction rate, v, extracted from demixing experiments plots versus polysaccharide concentration.

the creaming of flocculated droplets. Several scans in the z-direction were conducted to verify the formation of an interconnected network. The resulting micrograph (Fig. 6) shows that oleosome aggregates formed a 3D network when alginate at 0.025 wt% was added. Alginate-mediated clusters can be interpreted and cartooned in Fig. 7, which shows the behavior on different scales.

The estimates of the chain lengths and general properties of the molecular weight distribution of alginate (Kong et al., 2004; Martinsen et al., 1991) indicate that longer alginate chains can join two or more oleosomes. This will depend on the chain and block lengths for the uncharged units at certain concentrations. The fraction of longer chains form entanglements and provides additional stability to the aggregates (Fig. 7a). These partially covered oleosomes can form small aggregates, which join into larger clusters (Fig. 7b). Thus, the clusters can form alginate-mediated soft particle networks (Fig. 7c).

For >0.025 wt% alginate, microscopic images (Fig. 5 d-f) show that clusters become smaller as alginate content increases. Accordingly, the peak around 10 μm decreased, and the peak around 0.350 μm increased, which corresponds to intact oleosome droplets (Fi. 5f). The disappearance of these big clusters is also related to the decrease in v and B, and are visually reflected in the disappearance of transparent supernatant at 0.125 wt% alginate (Fig. 3a). This behavior suggests that oleosome droplets start to be re-stabilized by the increasing amount of alginate polymer chains. It is likely that at >0.125 wt% alginate, the concentration is sufficient to cover the droplet surfaces. This behavior is typical for interacting flexible polysaccharides which increase the stability of protein-coated oil droplets by forming protective interfacial multilayers (Bertsch et al., 2019).

Demixing in xanthan-oleosome mixtures presented a different behavior (Fig. 3b). At zero xanthan concentration, a homogeneous sample was observed (Fig. 8A), and no serum separation was observed within the first minutes. When xanthan was present at low concentrations, serum separation started early in the first minutes after preparation (Fig. 3b, d). In microscopy images, it can be observed that slightly flocculated oleosome droplets and the presence of large and irregularly shaped structures become more noticeable as xanthan content increases (Fig. 8c–f). In confocal microscopy pictures (Fig. 9a and b), xanthan 0.05 wt% showed similar irregularly shaped structures as observed in both 2D and 3D projection scans. It is well documented that xanthan induces microscopic and macroscopic phase separation when in combination with other colloidal systems (Hege et al., 2020; Ye et al., 2004). Depletion flocculation phenomena and geometric incompatibility are possible mechanisms that could lead to phase separation (Assenza & Mezzenga, 2019; Bhat et al., 2006; Bressel et al., 2020). Xanthan

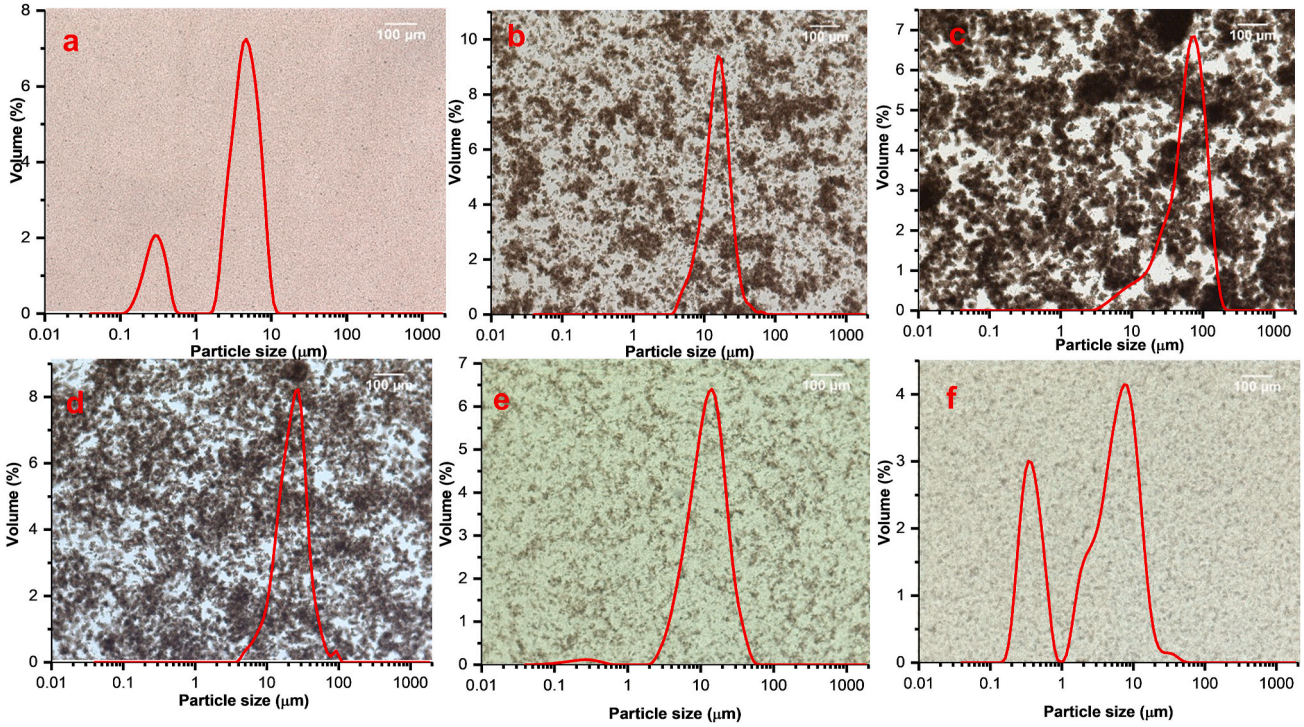

Fig. 5. Optical microscopy images Oleosome 5 wt% + Alginate after being adjusted to pH 4 combined with Particle size distributions of the same sample. a) 5 wt% Oleo- 0 wt% Alg b) 5 wt% Oleo- 0.0025 wt% Alg c) 5 wt% Oleo- 0.025 wt% Alg d) 5 wt% Oleo- 0.01 wt% Alg e) 5 wt% Oleo- 0.125 wt% Alg f) 5 wt% Oleo- 0.175 wt % Alg.

Table 2
Data parameters obtained from demixing plots. 5 wt% Oleosome. B is permeability coefficient and t_{delay} is delay time.

Mixture Oleosome/Polysaccharide	B (μm^2)	t_{delay} (min)
Sodium alginate		
0.0025 wt%	1580.44	10
0.025 wt%	7429.42	5
0.05 wt%	773.64	100
0.125 wt%	0	15,700
Xanthan gum		
0.0025 wt%	1105.20	20
0.025 wt%	1013.10	25
0.05 wt%	729.43	40
0.125 wt%	135.08	140

promotes flocculation by a depletion mechanism in which xanthan molecules are not entirely absorbed at the particle interface but are partially repelled from the region between the droplets. This causes the droplets to continue to approach each other, resulting in weak aggregation. However, interactions between the oleosome surface and the xanthan molecules occurred, albeit not extensively as observed in the ζ-potential values (Fig. 1b). Similarly, confocal microscopy images show that xanthan can interact with oleosome surfaces as observed by the white arrows in Fig. 9a. These arrows depict increased intensity in fluorescence which may indicate oleosomes droplets on the borders of xanthan molecules.

This limited interaction between xanthan and oleosome droplets may discard depletion as the primary mechanism for flocculation in this system. It is more likely that xanthan gum induces phase separation due to geometric incompatibility. Phase separation can readily occur in a binary mixture of isotropic particles (such as spherical oleosome droplets) and anisotropic particles (such as rod-like xanthan molecules) (Koczo et al., 1998). This incompatibility becomes more favorable than electrostatic interactions and becomes more pronounced when the length-to-diameter ratio of the rods increases, as in the case of xanthan

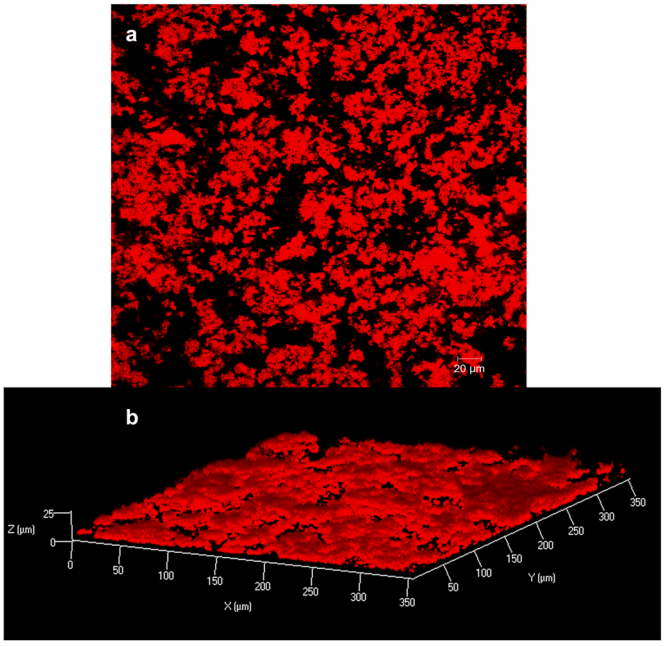

Fig. 6. CLSM images of a) 5 wt% Oleosome with 0.025 wt% Alginate b) z-scan surface plot of sample 5 wt% Oleosome- 0.025 wt% Alginate. To visualize droplet aggregates for CLSM, samples were stained with Nile Red which dyes the oil core. (For interpretation of the references to colour in this figure legend, the reader is referred to the Web version of this article.)

gum. Xanthan-induced-phase separation caused by geometric incompatibilities agrees with earlier theories (Koczo et al., 1998). However, the presence of loose oleosome aggregates in xanthan-containing mixtures questions whether this flocculation is due to depletion mechanisms to a certain extent. Usually, when particles are flocculated due to

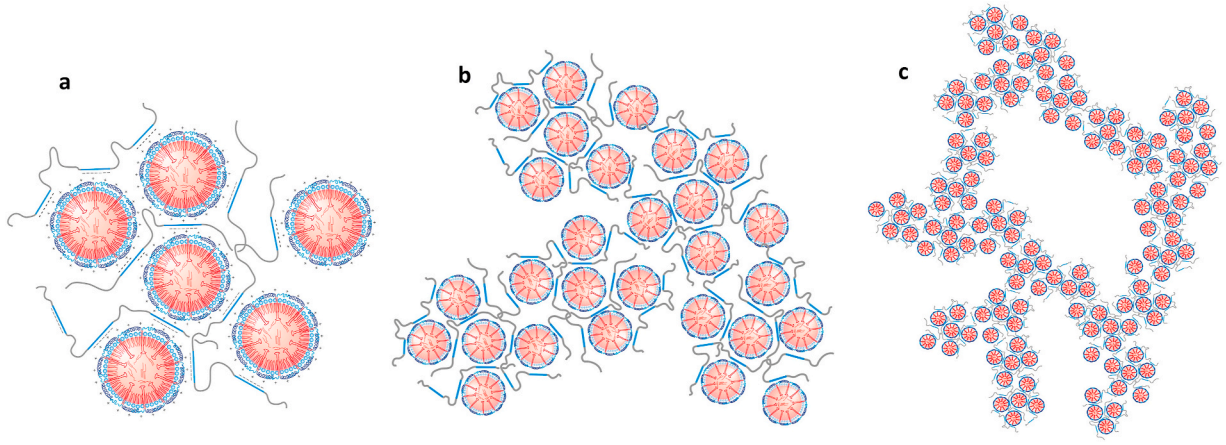

Fig. 7. The bridging flocculation at 0.025 wt% alginate 5% Oleosome. (a) The oleosomes are coated partly by the negative charged blocks of the polymer. Entanglement formation between oleosomes become more likely, when chains are sufficiently long, i.e., by the high molecular weight fraction. (b) Oleosome aggregated are able to form larger clusters, which are able to join to a soft oleosome particle gel (c).

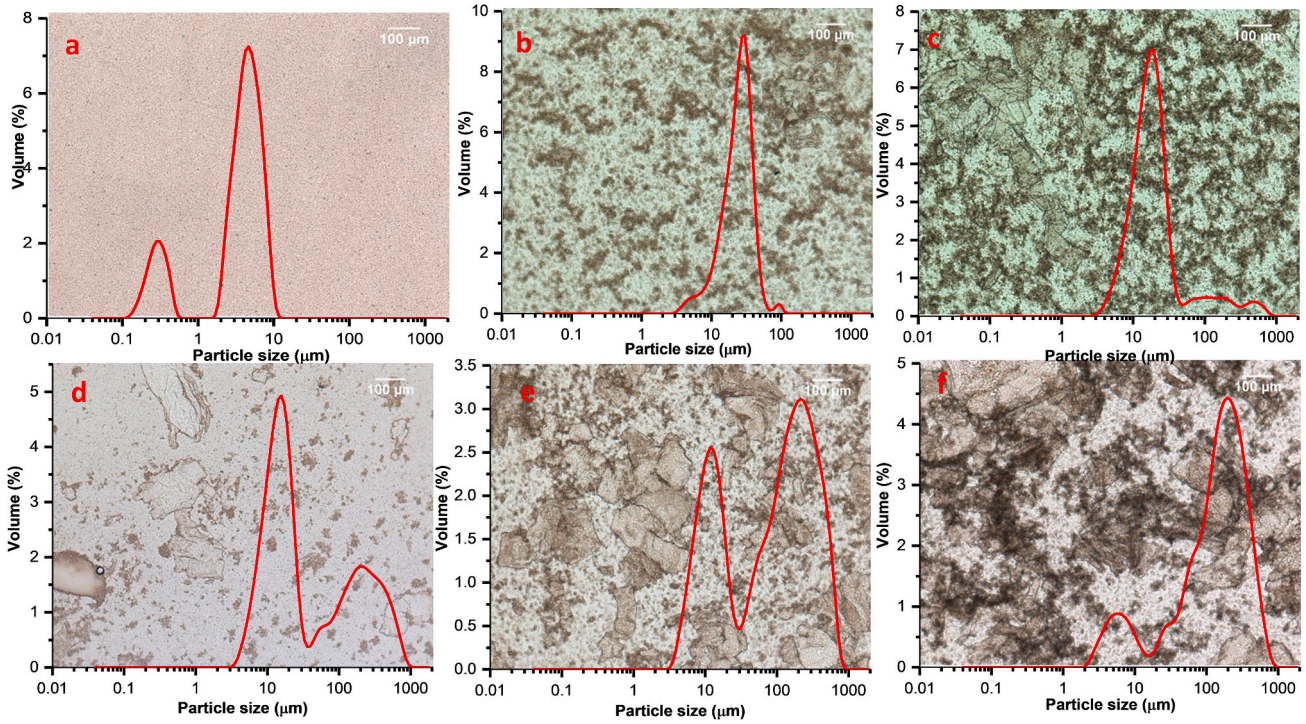

Fig. 8. Optical microscopy images Oleosome 5 wt% + Xantham gum after being adjusted to pH 4 combined with Particle size distributions of the same sample. a) 5 wt% Oleo- 0 wt% Xanthan b) 5 wt% Oleo- 0.0025 wt% Xanthan c) 5 wt% Oleo- 0.025 wt% Xanthan d) 5 wt% Oleo- 0.01 wt% Xanthan e) 5 wt% Oleo- 0.125 wt% Xanthan f) 5 wt% Oleo- 0.175 wt% Xanthan.

depletion by a polymer, a particle network is formed (Souza et al., 2019).

3.2.2. *Effect of xanthan concentration on flocculation behavior*

A delay time, $t_{delay,}$ in supernatant separation was present in xanthan-containing mixtures and it increased at increasing xanthan concentrations, as observed in Table 2. This behavior is consistent with previous studies where high xanthan concentrations delayed the creaming of oil droplets (Ye et al., 2004). It is likely that the large xanthan molecules, as xanthan content increases, generate a viscosity increase in the aqueous phase.

Delay time in emulsions flocculated by non-adsorbing polysaccharides has been found to scale with the aqueous phase shear viscosity, the density difference between the oil and the aqueous phase, and permeability as $t_{delay} \sim B^{-1}\eta\Delta\rho^{-1}$ (T. B. Blijdenstein, Van Winden, et al., 2004). Therefore, the delay time in xanthan-containing mixtures is given by the combined effect of viscosity in the continuous phase and the permeability in the droplet network. The pores within the droplet network may be too small in the first minutes to allow supernatant separation. Eventually, the pores become wider by the effect of structural rearrangements driven by gravity. This is counteracted by the viscous drag of the aqueous phase, which hinders the upward movement of droplets, and it is in agreement with v, which decreases with xanthan content. Characteristic concentrations for xanthan are critical overlap concentration (c^*) of 0.007 wt% (Vilgis, 2015) and entanglement concentration c_e of 0.01 wt% (Rodd et al., 2000). As a result, it is likely that xanthan, at the conditions above, is in the overlap regime. Therefore, viscosity in the continuous phase plays a critical role in the phase

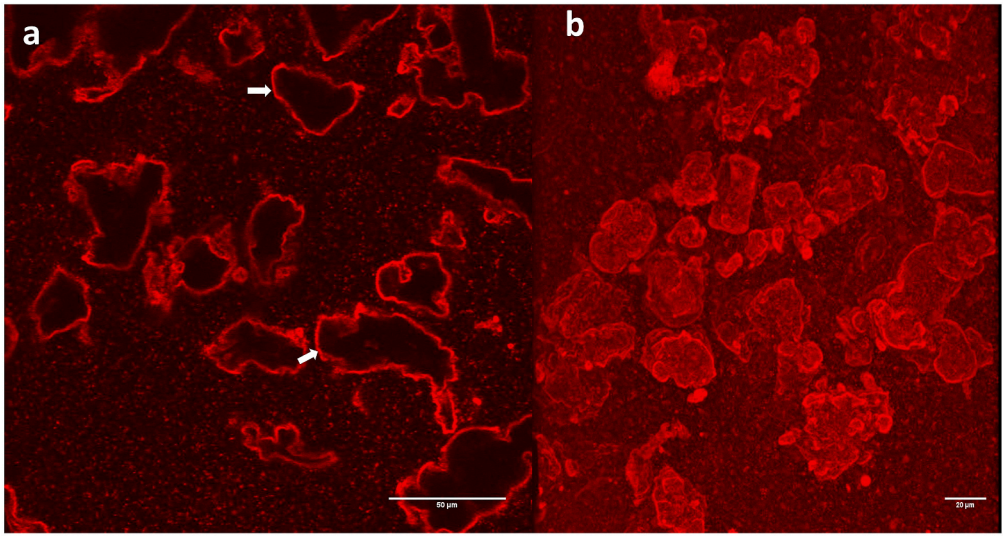

Fig. 9. Confocal micrographs of a) 5 wt% Oleosome- 0.05 wt% Xanthan. White arrows indicate presence of oil bodies at the interface of xanthan molecules b) 3D Project of sample 5 wt% Oleosome- 0.05 wt% Xanthan.

separation dynamics of xanthan-containing mixtures. Compared with 0.0025 wt% alginate, which presents v 3.90 mm/h, 0.0025 wt% xanthan presents lower v, 0.0045 mm/h, while both present similar B, 1580.44 μm^2 and 1105.20 μm^2, respectively. This means that despite showing similar network porosity (due to droplet flocculation), the flocculation rate is slower in xanthan due to its influence in the higher viscosity of the continuous phase. This suggest that the effect of xanthan on the phase separation dynamics arises from the competing effects xanthan concentration has on geometrical incompatibility and bulk viscosity. At low xanthan concentrations (0.0025 wt %- 0.05 wt %), flocculation dynamics are dominated by the effect of geometrical incompatibility, which causes microscopic and macroscopic phase separation. At higher xanthan concentrations (>0.125 wt %), macroscopic phase separation slows due to the slower droplet dynamics caused by the increasing viscosity of the xanthan-rich continuous phase.

3.2.3. *Effect of alginate/oleosome ratio on bridging flocculation*

Fig. 10a shows a maximum in apparent d_{43} as a function of alginate concentration at three oleosome concentrations. This maximum value occurred at the alginate concentration, which induced maximum bridging flocculation. These maximum values are plotted as a function of oleosome concentration (Fig. 10b), resulting in an almost perfect linear relation. This linear relation indicates that the amount of alginate to induce maximum aggregation is proportional to the surface area of the oleosome. The plot slope is 0.005, indicating a relationship of $\%c_{Alg} = 0.005 \times \%c_{Oleo}$. Interestingly, d_{43} exhibits a sharp peak at 0.005 when plotted as a function of the polysaccharide/oleosome ratio (Fig. 10c), which is the same value as the slope of the linear fitting. Therefore, the alginate concentration for inducing maximum bridging flocculation is linearly dependent on the oleosome concentration making the ratio between alginate and oleosome a critical condition for inducing extensive flocculation. The dependence on the polymer and particle ratio for inducing maximum flocculation if the polymer is adsorptive to the particle is characteristic of bridging flocculation mechanism. The optimum ratio between alginate polymer chains and oleosome droplets for bridging flocculation corresponds to an interfacial coverage of approximately 0.4 mg/m^2. This value is similar to those found for other anionic polysaccharides that induced bridging flocculation in protein-coated oil droplets: approximately 1 mg/m^2 for carrageenan and carboxymethylcellulose (T. Blijdenstein, Van Winden, et al., 2004a,b; Dickinson & Pawlowsky, 1998) and 0.2–0.3 mg/m^2 for dextran sulfate (Dickinson & Pawlowsky, 1996). The fact that optimum bridging in alginate was closer to the values reported for dextran sulfate suggests that charge density in polysaccharides plays a critical role in bridging flocculation. Dextran sulfate is a highly charged density polysaccharide that adsorbs to a protein-coated surface even at neutral pH values. Similarly, as observed in Fig. 1a, alginate adsorbed to the oleosome surface at pH 6.00.

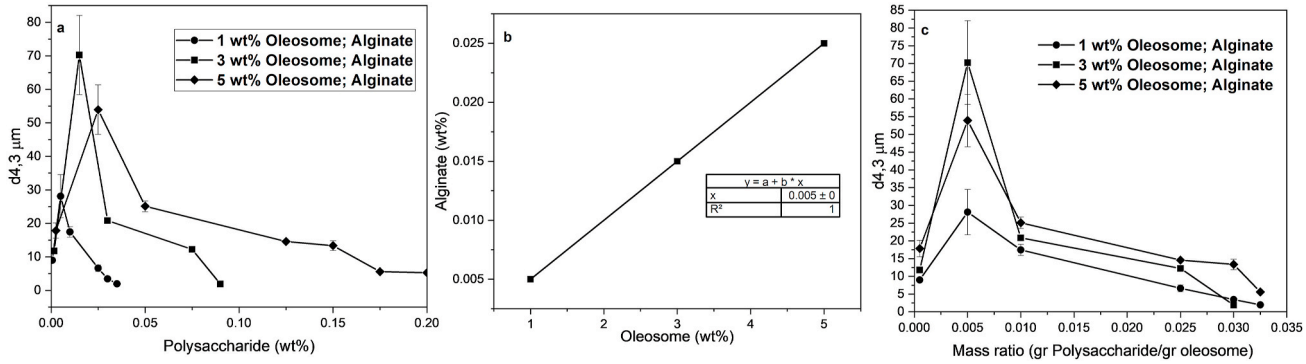

Fig. 10. a) Mean particle size (d_{43}) as a function of Alginate concentration at three different Oleosome concentrations b) Plot showing alginate concentration (wt %) at maximum aggregation as function of oleosome (wt %) and an insert showing linear fitting and its parameters c) Mean particle size (d_{43}) from an expressed as a function of Polysaccharide/Oleosome mass ratio at three different Oleosome concentrations.

3.2.4. Xanthan-oleosome flocculation mechanism

Xanthan, on the other hand, despite being an anionic polysaccharide, showed a different flocculation mechanism. As observed in the previous experiments, Fig. 11 shows a different flocculation mechanism in xanthan. Instead of showing a maximum particle size, it shows a gradual increase in d_{43} with an increasing concentration of xanthan (Fig. 11). This increase in d_{43} increase are in accordance to the large irregular structures observed in optical microscopy images (Fig. 8) which seem to become predominant as the xanthan content increases. It is proposed that these large structures, also observed in confocal images (Fig. 9), correspond to xanthan molecules that separate into local microdomains because it becomes more favorable than interacting with oleosome droplets.

The partial demixing in the xanthan-oleosome mixtures can be understood by considering two driving forces: Firstly, since xanthan is strongly electrostatically negatively charged, the strongly repulsive and rigid molecules can only assume very specific conformations in the dissolved state. Liquid crystalline structures are excluded because of the strong repulsion. Consequently, compromises have to be made because of the repulsion. Therefore, xanthan molecules orient themselves randomly to minimize electrostatic energy and maximize entropy (Nordqvist & Vilgis, 2011). The second point is the low adsorption tendency of the xanthan molecules on the surfaces of the oleosomes, already indicated in Fig. 2, which is also due to the high chain rigidity.

As a consequence of the electrostatic attraction, xanthan-mediated aggregates of oleosomes can form, but these have a much poorer cohesion than those with alginate. Clustering, or even the formation of a particle network, as indicated in Fig. 7, is largely excluded. For entropic and energetic reasons, only more narrowly confined domains of oleosome-xanthan phases remain stable. hile the xanthan molecules not adsorbed (on oleosomes) separate from them, as shown in the red and black regions by confocal microscopy shown in Fig. 9b. These considerations lead to the model shown in Fig. 12.

An additional limiting factor in the size of the xanthan oleosome aggregate is their net surface charge, which depends on the local arrangement between xanthan and oleosomes. The larger the aggregates are, the larger becomes their net surface charge. Rayleigh instabilities will limit the size of the loosely bound aggregates (Deserno, 2001; Taflin et al., 1989), another factor of provoking depletion flocculation.

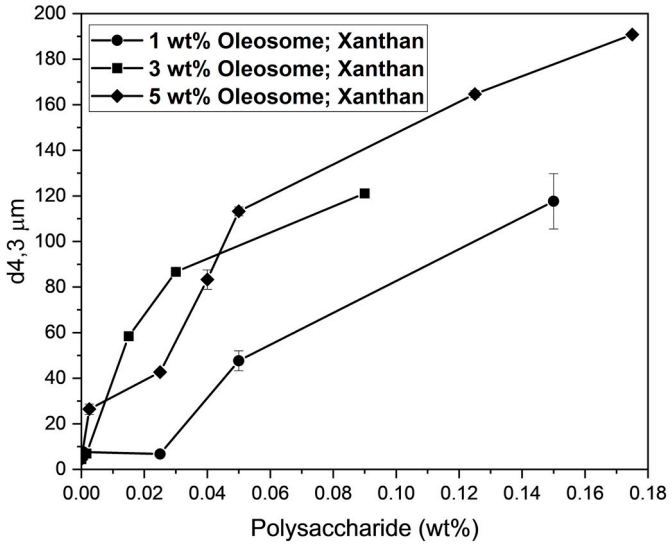

Fig. 11. Mean particle size (d_{43}) as a function of Xanthan concentration at three different Oleosome concentrations.

3.3. Characterization of compacted gels obtained upon densification of flocculated emulsions

Flocculated polysaccharide-oleosome mixtures were centrifuged to compact the droplet network and analyze the resulting materials. As observed in Fig. 13b, alginate-containing mixtures at optimum bridging ratio (0.005 g/g) presented a compact and self-supporting gel upon centrifugation, which corresponds to an oleosome content of about 46 wt%. Fig. 14 showed that higher and lower alginate/oleosome ratios resulted in either more turbid supernatant or lesser compact gels, which indicated that polymer bridging became less effective.

3.3.1. Rheological characterization of resulting materials

Fig. 12a shows the dependence on polysaccharide/oleosome mass ratio of compacted gels with the storage modulus G' given by oscillatory rheological measurements. There is a steep increase in G' up to 8000 Pa at 0.005 g alginate/g oleosome followed by a drop at higher ratios. This maximum G' at optimum bridging ratio confirms that this ratio is fully consistent with forming a network of polymer cross-linked droplets. At increased alginate ratios, a re-stabilization occurs, and the system becomes less elastic. Fig. 14a shows the amplitude sweep plots for compacted gels at the optimum bridging ratio (0.005 g/g) and 0.025 g/g, corresponding to the re-stabilization of oleosome droplets. At optimum bridging, the modulus is constant up to 10% strain and shows a sudden decrease at larger strains. This sudden decrease is indicative of a microscopic fracture of the gel, and it is typical of bridging-flocculated gels (T. B. Blijdenstein, Van Winden, et al., 2004a,b). Although 0.025 g/g alginate shows a decrease of G' due to droplet re-stabilization, it still shows a gel-like response $G' > G''$ suggesting the system might still present polysaccharide bridges. This indicates that the rheological properties of polymer-bridging gels can be tuned by varying alginate/oleosome ratios. Alginate/oleosome ratios close to optimum bridging (0.005 g/g) will yield compact and stiffer gels, while ratios far from the optimum ratio will yield less compact and softer gels as the number of polymer bridges may decrease.

On the other hand, the addition of xanthan did not present a transparent supernatant at any given ratio after centrifugation (Fig. 15). When removed, the cream did not show a compact gel, but had the characteristics of a viscous cream. Rheological measurements of the collected cream suggest that the rheological response is most likely given by oleosome droplets alone since there was no significant difference in G' at the different xanthan/oleosome ratios (Fig. 13a). This confirms that polysaccharide bridges are not present at a given xanthan content. This observation is supported in Fig. 15, where at 0.025 g/g can be observed the presence of sediment at the bottom of the tube. This sediment suggests that xanthan molecules were present in the continuous phase allowing them to be easily precipitated. This observation is consistent with the results of the previous sections that xanthan gum induces microscopic phase separation, with this effect becoming more pronounced with increasing xanthan concentration.

These results are strongly supported by the models presented so far. The linear modulus G' of the alginate-oleosome mixture at the optimum bridging flocculation ratio is about two orders of magnitude higher than the xanthan oleosome solution at the corresponding concentration. Moreover, Fig. 7 shows a higher concentration dependence for alginate than for xanthan. The high modulus for alginate-oleosome mixtures supports the idea of forming a particle-cluster network as drawn in Fig. 7c. The interconnected network, as confirmed by CLSM, carries stresses and shear up to 10% deformation before the particle gel ruptures to sub-units. Then the storage modulus G' drops. It decreases as expected for larger ratios of the alginate–oleosome mixtures. Many oleosomes are already sufficiently covered with alginate; inter-oleosome bridging can no longer form on large scales. Therefore the network becomes weaker. Similar arguments explain the shorter linear viscoelastic (LVE) range for the higher concentrations. The weaker network

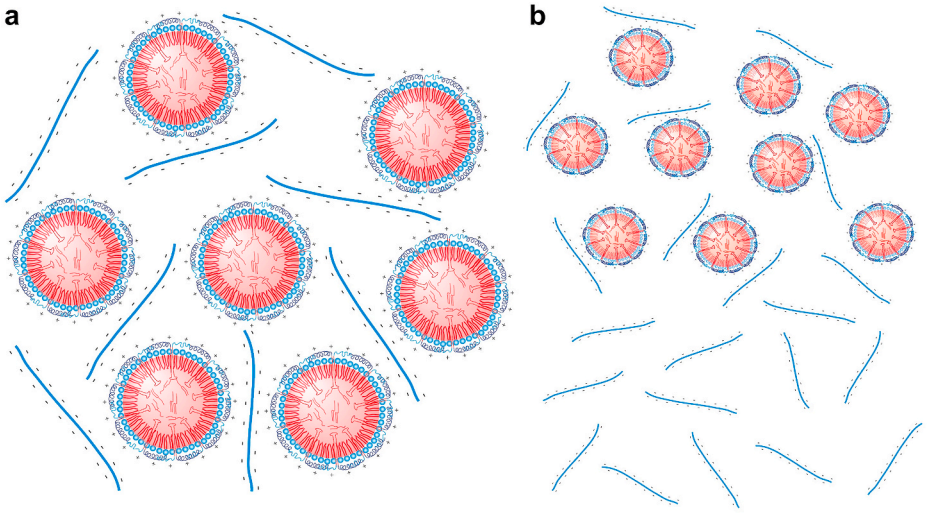

Fig. 12. Small droplets in between xanthan form loosely bound aggregates (a). Only a small number of xanthan molecules can adsorb on the oleosome surfaces. The aggregates are not stable at larger size, therefore a depletion flocculation occurs (b).

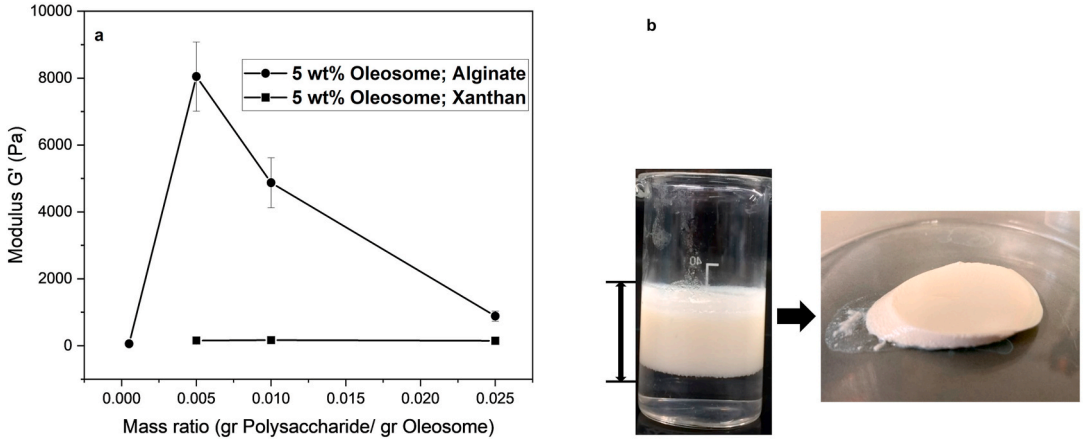

Fig. 13. a) Plots of G′ at 1% strain as a function of mass ratio for 5 wt% Oleosome b) Before (5 wt % Oleosome) and after Centrifugation (45 wt %) of 0.005 g/g Alginate showing a compact self-supporting gel.

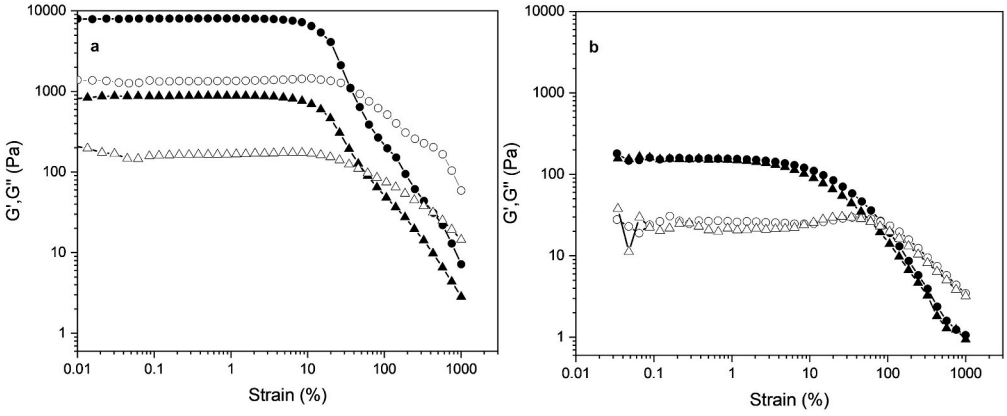

Fig. 14. Oscillatory amplitude sweeps of compacted gels Oleosome content 46 wt% at two fixed polysaccharide/oleosome ratios 0.005 g/g (●) and 0.025 g/g (▲) of a) alginate and b) xanthan. G': filled symbols, G'': open symbols.

disintegrates at lower deformations. The larger LVE range supports the presence of entanglements (compare Fig. 7a), which makes the densified samples more rubbery.

The relatively low modulus xanthan solutions are also in line with the model proposed in Fig. 12. The cohesion of the clusters is significantly weaker, and the flocculated and densified solution does not support large deformation. Therefore, the LVE range becomes smaller compared to the alginate solutions. Likewise, the more pronounced

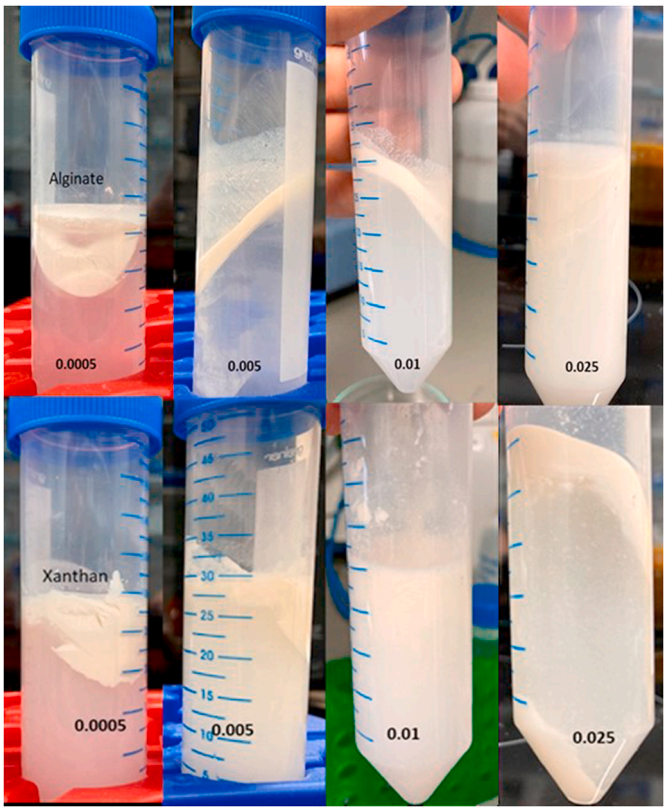

Fig. 15. Flocculated oleosome emulsions upon centrifugation which depicts separation between supernatant and compacted cream network.

hump in the loss modulus G'' is noticeable for deformations around 80%–100%. Xanthan molecules become arrested in a randomly oriented state at higher concentrations and form a stable pseudo-gel (Vilgis, 2015). Each highly stiff, rod-like molecule is stuck in a cage formed by the surrounding charged polymers and oleosomes, and only local motions and limited rotations are possible. Only higher shear deformations orient the molecules in the direction of the shear, and large-scale motion becomes possible. The slight increase of G'' can thus be attributed to the overcoming of the electrostatic energy of the cage. The almost parallel motion of the xanthan molecules requires only little energy and stress, the solution flows, and the loss modulus decreases further.

4. Conclusions

This study reports the gelation of oleosome emulsions using bridging flocculation as a structuring mechanism. Polysaccharides' ability to induce bridging flocculation will depend on the configuration properties of the polymer chain, interaction strength between polysaccharide-oleosome, and the polysaccharide-oleosome concentration ratio. Polysaccharides with flexible polymer chains, such as alginate, will be effective for bridging since charged blocks of the chain will adsorb efficiently on the oleosome surface via strong electrostatic interactions. Polysaccharides with semi-flexible, almost stiff chains, such as xanthan, cannot effectively interact with the oleosome surface due to energy constraints given by its rigidity. As a result, xanthan leads to a depletion effect where phase separation occurs at different scales between xanthan and oleosomes. Alginate-driven bridging occurs efficiently at an optimum polysaccharide-oleosome concentration ratio, expressed as 0.005 g/g or 0.4 mg/m^2. This optimum ratio is characterized by an interconnected and dense droplet network, as confirmed by rheology and confocal microscopy measurements. Upon densification, bridging-flocculated emulsions lead to a compact and self-supporting soft gel characterized by fracture behavior at higher strains in oscillatory rheology. This densification process resulted in gels of about 46 wt% oleosome starting from 5 wt% oleosome. This diversity in varying oleosome concentrations and polysaccharide-oleosome ratios provides opportunities to tune network structure and its resulting rheological properties. Generally overlooked as a gelation mechanism, bridging flocculation can be further exploited as a gelation method due to a straightforward preparation method that requires small amounts of polysaccharides and oleosome emulsion.

Credit author statement

Juan Carlos Zambrano. Conceptualization, methodology, acquisition of data, analysis and/or interpretation of data, writing original draft. Thomas A. Vilgis. Supervision, conceptualization, writing – review and editing, visualization, and interpretation.

Conflicts of interest statement

We certify that the authors have no affiliations with or involvement in any organization or entity with any financial interest (such as honoraria; educational grants; participation in speakers' bureaus; membership, employment, consultancies, stock ownership, or other equity interest; and expert testimony or patent-licensing arrangements), or non-financial interest (such as personal or professional relationships, affiliations, knowledge or beliefs) in the subject matter or materials discussed in this manuscript.

Data availability

Data will be made available on request.

References

Assenza, S., & Mezzenga, R. (2019). Soft condensed matter physics of foods and macronutrients. *Nature Reviews Physics, 1*(9), 551–566. https://doi.org/10.1038/s42254-019-0077-8

Bastos, L. P. H., de Carvalho, C. W. P., & Garcia-Rojas, E. E. (2018). Formation and characterization of the complex coacervates obtained between lactoferrin and sodium alginate. *International Journal of Biological Macromolecules, 120*, 332–338. https://doi.org/10.1016/j.ijbiomac.2018.08.050

Bertsch, P., Thoma, A., Bergfreund, J., Geue, T., & Fischer, P. (2019). Transient measurement and structure analysis of protein–polysaccharide multilayers at fluid interfaces. *Soft Matter, 15*(31), 6362–6368. https://doi.org/10.1039/C9SM01112A

Bhat, S., Tuinier, R., & Schurtenberger, P. (2006). Spinodal decomposition in a food colloid–biopolymer mixture: Evidence for a linear regime. *Journal of Physics: Condensed Matter, 18*(26), L339. https://doi.org/10.1088/0953-8984/18/26/L01

Blijdenstein, T., Van Winden, A., Van Vliet, T., Van der Linden, E., & Van Aken, G. (2004a). Serum separation and structure of depletion-and bridging-flocculated emulsions: A comparison. *Colloids and Surfaces A: Physicochemical and Engineering Aspects, 245*(1–3), 41–48. https://doi.org/10.1016/j.colsurfa.2004.07.002

Blijdenstein, T. B., van der Linden, E., van Vliet, T., & van Aken, G. A. (2004b). Scaling behavior of delayed demixing, rheology, and microstructure of emulsions flocculated by depletion and bridging. *Langmuir, 20*(26), 11321–11328. https://doi.org/10.1021/la048608z

Boonlao, N., Shrestha, S., Sadiq, M. B., & Anal, A. K. (2020). Influence of whey protein-xanthan gum stabilized emulsion on stability and in vitro digestibility of encapsulated astaxanthin. *Journal of Food Engineering, 272*, Article 109859.

Bressel, K., Muller, W., Leser, M. E., Reich, O., Hass, R., & Wooster, T. J. (2020). Depletion-induced flocculation of concentrated emulsions probed by photon density wave spectroscopy. *Langmuir, 36*(13), 3504–3513. https://doi.org/10.1021/acs.langmuir.9b03642

Cheng, H., & Olvera de la Cruz, M. (2003). Adsorption of rod-like polyelectrolytes onto weakly charged surfaces. *Journal of Chemical Physics, 119*(23), 12635–12644. https://doi.org/10.1063/1.1626630

De Gennes, P.-G. (1979). *Scaling concepts in polymer physics*. Cornell university press.

Deserno, M. (2001). Rayleigh instability of charged droplets in the presence of counterions. *The European Physical Journal E, 6*(2), 163–168. https://doi.org/10.1007/s101890170018

Dickinson, E., & Pawlowsky, K. (1996). Effect of high-pressure treatment of protein on the rheology of flocculated emulsions containing protein and polysaccharide. *Journal of Agricultural and Food Chemistry, 44*(10), 2992–3000. https://doi.org/10.1021/jf960188z

Dickinson, E., & Pawlowsky, K. (1997). Effect of ι-carrageenan on flocculation, creaming, and rheology of a protein-stabilized emulsion. *Journal of Agricultural and Food Chemistry, 45*(10), 3799–3806. https://doi.org/10.1021/jf970304d

Dickinson, E., & Pawlowsky, K. (1998). Influence of κ-carrageenan on the properties of a protein-stabilized emulsion. *Food Hydrocolloids, 12*(4), 417–423. https://doi.org/10.1016/S0268-005X(98)00055-1

Eremin, Y. (2004). Scattering: Scattering theory. Five-Volume Set. In *Encyclopedia of modern optics* (pp. 326–330).

Hege, J., Palberg, T., & Vilgis, T. A. (2020). Interactions of different hydrocolloids with milk proteins. *Journal of Physics: Materials, 3*(4), Article 044003. https://doi.org/10.1088/2515-7639/aba2b7

Huang, A. H. (1992). Oil bodies and oleosins in seeds. *Annual Review of Plant Biology, 43*(1), 177–200. https://doi.org/10.1146/annurev.pp.43.060192.001141

Hu, C., Lu, W., Mata, A., Nishinari, K., & Fang, Y. (2021). Ions-induced gelation of alginate: Mechanisms and applications. *International Journal of Biological Macromolecules, 177*, 578–588. https://doi.org/10.1016/j.ijbiomac.2021.02.086

Jiang, X., Li, Y., Tang, X., Jiang, J., He, Q., Xiong, Z., & Zheng, H. (2021). Biopolymer-based flocculants: A review of recent technologies. *Environmental Science and Pollution Research, 28*(34), 46934–46963. https://doi.org/10.1007/s11356-021-15299-y

Koczo, K., Wasan, D. T., Borwankar, R. P., & Gonsalves, A. (1998). Flocculation of food dispersions by gums: Isotropic/anisotropic dispersion separation by xanthan gum. *Food Hydrocolloids, 12*(1), 43–53. https://doi.org/10.1016/S0268-005X(98)00044-7

Kong, H. J., Kaigler, D., Kim, K., & Mooney, D. J. (2004). Controlling rigidity and degradation of alginate hydrogels via molecular weight distribution. *Biomacromolecules, 5*(5), 1720–1727. https://doi.org/10.1021/bm049879r

Martinsen, A., Skjak-Braek, G., Smidsrod, O., Zanetti, F., & Paoletti, S. (1991). Comparison of different methods for determination of molecular weight and molecular weight distribution of alginates. *Carbohydrate Polymers, 15*(2), 171–193. https://doi.org/10.1016/0144-8617(91)90031-7

Moorhouse, R., Walkinshaw, M., & Arnott, S. (1977). *Xanthan Gumâ€" molecular conformation and interactions*. ACS Publications. https://doi.org/10.1021/bk-1977-0045.ch007

Moschakis, T., Murray, B. S., & Dickinson, E. (2006). Particle tracking using confocal microscopy to probe the microrheology in a phase-separating emulsion containing nonadsorbing polysaccharide. *Langmuir, 22*(10), 4710–4719. https://doi.org/10.1021/la0533258

Nikiforidis, C. V. (2019). Structure and functions of oleosomes (oil bodies). *Advances in Colloid and Interface Science, 274*, Article 102039. https://doi.org/10.1016/j.cis.2019.102039

Nikiforidis, C. V., & Kiosseoglou, V. (2010). Physicochemical stability of maize germ oil body emulsions as influenced by oil body surface− xanthan gum interactions. *Journal of Agricultural and Food Chemistry, 58*(1), 527–532. https://doi.org/10.1021/jf902544j

Nordqvist, D., & Vilgis, T. A. (2011). Rheological study of the gelation process of agarose-based solutions. *Food Biophysics, 6*(4), 450–460. https://doi.org/10.1007/s11483-011-9225-0

Payne, L., Rodrigues, J., & Straughan, B. (2001). Effect of anisotropic permeability on Darcy's law. *Mathematical Methods in the Applied Sciences, 24*(6), 427–438. https://doi.org/10.1002/mma.228

Qi, B., Ding, J., Wang, Z., Li, Y., Ma, C., Chen, F., Sui, X., & Jiang, L. (2017). Deciphering the characteristics of soybean oleosome-associated protein in maintaining the stability of oleosomes as affected by pH. *Food Research International, 100*, 551–557. https://doi.org/10.1016/j.foodres.2017.07.053

Rodd, A., Dunstan, D., & Boger, D. (2000). Characterisation of xanthan gum solutions using dynamic light scattering and rheology. *Carbohydrate Polymers, 42*(2), 159–174. https://doi.org/10.1016/S0144-8617(99)00156-3

Sato, T., Kakihara, T., & Teramoto, A. (1990). Isotropic-liquid crystal phase equilibrium in semiflexible polymer solutions: Xanthan, a rigid polyelectrolyte. *Polymer, 31*(5), 824–828. https://doi.org/10.1016/0032-3861(90)90041-V

Souza, S. F., Mariano, M., De Farias, M. A., & Bernardes, J. S. (2019). Effect of depletion forces on the morphological structure of carboxymethyl cellulose and micro/nano cellulose fiber suspensions. *Journal of Colloid and Interface Science, 538*, 228–236. https://doi.org/10.1016/j.jcis.2018.11.096

Su, C., Feng, Y., Ye, J., Zhang, Y., Gao, Z., Zhao, M., Yang, N., Nishinari, K., & Fang, Y. (2018). Effect of sodium alginate on the stability of natural soybean oil body emulsions. *RSC Advances, 8*(9), 4731–4741. https://doi.org/10.1039/C7RA09375F

Taflin, D. C., Ward, T. L., & Davis, E. J. (1989). Electrified droplet fission and the Rayleigh limit. *Langmuir, 5*(2), 376–384.

Ting, J. T., Lee, K., Ratnayake, C., Platt, K. A., Balsamo, R. A., & Huang, A. H. (1996). Oleosin genes in maize kernels having diverse oil contents are constitutively expressed independent of oil contents. *Planta, 199*(1), 158–165. https://doi.org/10.1007/BF00196892

Tzen, J. T., Cao, Y., Laurent, P., Ratnayake, C., & Huang, A. H. (1993). Lipids, proteins, and structure of seed oil bodies from diverse species. *Plant Physiology, 101*(1), 267–276. https://doi.org/10.1104/pp.101.1.267

Vilgis, T. A. (2015). Gels: Model systems for soft matter food physics. *Current Opinion in Food Science, 3*, 71–84. https://doi.org/10.1016/j.cofs.2015.05.009

Wang, A., & Wang, W. (2013). Gum-g-copolymers: Synthesis, properties, and applications. In *Polysaccharide based graft copolymers* (pp. 149–203). Springer.

Waschatko, G., Schiedt, B., Vilgis, T. A., & Junghans, A. (2012). Soybean oleosomes behavior at the air–water interface. *The Journal of Physical Chemistry B, 116*(35), 10832–10841. https://doi.org/10.1021/jp211871v

Yang, N., Feng, Y., Su, C., Wang, Q., Zhang, Y., Wei, Y., Zhao, M., Nishinari, K., & Fang, Y. (2020). Structure and tribology of κ-carrageenan gels filled with natural oil bodies. *Food Hydrocolloids, 107*, Article 105945. https://doi.org/10.1016/j.foodhyd.2020.105945

Ye, A., Hemar, Y., & Singh, H. (2004). Enhancement of coalescence by xanthan addition to oil-in-water emulsions formed with extensively hydrolysed whey proteins. *Food Hydrocolloids, 18*(5), 737–746. https://doi.org/10.1016/j.foodhyd.2003.11.010

Yu, X., & Somasundaran, P. (1996). Role of polymer conformation in interparticle-bridging dominated flocculation. *Journal of Colloid and Interface Science, 177*(2), 283–287. https://doi.org/10.1006/jcis.1996.0033

Zhai, H., Gunness, P., & Gidley, M. J. (2021). Depletion and bridging flocculation of oil droplets in the presence of β-glucan, arabinoxylan and pectin polymers: Effects on lipolysis. *Carbohydrate Polymers, 255*, Article 117491. https://doi.org/10.1016/j.carbpol.2020.117491

Zhou, Y., & Franks, G. V. (2006). Flocculation mechanism induced by cationic polymers investigated by light scattering. *Langmuir, 22*(16), 6775–6786. https://doi.org/10.1021/la060281+

Zielbauer, B. I., Jackson, A. J., Maurer, S., Waschatko, G., Ghebremedhin, M., Rogers, S. E., Heenan, R. K., Porcar, L., & Vilgis, T. A. (2018). Soybean oleosomes studied by small angle neutron scattering (SANS). *Journal of Colloid and Interface Science, 529*, 197–204. https://doi.org/10.1016/j.jcis.2018.05.080